buildings

MDPI

Article

Compressive Test Investigation and Numerical Simulation of Polyvinyl-Alcohol (PVA)-Fiber-Reinforced Rubber Concrete

Yong Feng [1], Zijuan Niu [1], Chen Zhao [2] and Lijuan Li [1,*]

[1] College of Civil Engineering and Architecture, Henan University of Technology, Zhengzhou 450001, China
[2] Department of Hydraulic Engineering, Henan Vocational College of Water Conservancy and Environment, Zhengzhou 450008, China
* Correspondence: xgbllj2019117@haut.edu.cn

Abstract: To investigate the mechanical properties of polyvinyl-alcohol (PVA)-fiber-reinforced rubber concrete, 13 groups of PVA rubber/concrete specimens with PVA volume fractions of 0%, 0.5 vol%, 1.0 vol%, and 1.5 vol% and rubber particles with volume replacement sand ratios of 0%, 10%, 20%, and 30% were prepared, and the uniaxial compression full curve test was performed. The findings indicate that the bridging effect of PVA, as well as the synergistic effect of PVA and rubber particles, can improve the compressive properties of concrete, and the failure of the specimens demonstrates obvious ductile characteristics. Furthermore, PVA has a better impact on rubber concrete's bearing capacity, crack propagation of the failure surface, and compressive strength in the latter stages. PVA-fiber-reinforced rubber concrete is thought to be a six-phase composite made up of the aggregate phase, mortar matrix, PVA fiber, rubber particles, aggregate–mortar interface, and rubber–mortar interface on the mesoscale. To simulate the entire process of concrete with varying PVA rubber/content from integrity to damage and cracking, a meso-numerical model of PVA rubber/concrete was constructed. The simulation results and test results are in good agreement, demonstrating the validity of the mesomodel and offering a theoretical foundation for the structural analysis and design of this type of concrete.

Keywords: PVA fiber rubber/concrete; compression test; numerical simulation

Citation: Feng, Y.; Niu, Z.; Zhao, C.; Li, L. Compressive Test Investigation and Numerical Simulation of Polyvinyl-Alcohol (PVA)-Fiber-Reinforced Rubber Concrete. *Buildings* **2023**, *13*, 431. https://doi.org/10.3390/buildings13020431

Academic Editors: Bingxiang Yuan, Yong Liu, Xudong Zhang and Yonghong Wang

Received: 10 December 2022
Revised: 15 January 2023
Accepted: 19 January 2023
Published: 3 February 2023

1. Introduction

Rubber concrete, a brand new recycled building material for environmental protection, is created by combining waste rubber scraps with regular concrete. It significantly resolves the issue of environmental degradation and land occupation brought on by used tire rubber.

Instead of using aggregates, rubber particles can be used to enhance the toughness, freeze–thaw resistance, and energy absorption of regular concrete [1]. However, the reduced stiffness of rubber particles compared to regular concrete will result in a decrease in compressive strength. Elastic rubber deforms more under compression load than cement paste and speeds up the production of cracks [2,3]. Additionally, the tensile strength of regular concrete will decrease due to the low bonding strength of rubber particles at the interface with cement paste [4,5]. Although ordinary concrete with a high proportion of rubber aggregate reduces compressive strength, it can improve impact resistance and toughness by incorporating rubber aggregate [6]. Rubber tire recycling into Portland cement concrete can generally lessen environmental dangers and conserve natural resources. Fiber-reinforced concrete has benefits over conventional concrete such as crack prevention, improved flexural performance, and drying shrinkage inhibition [7–9]. PVA fiber was included in engineering cement composites (ECCs) by domestic and international scholars [10–12], who also extensively researched the performance of PVA-ECC [13]. PVA fiber was discovered to be one of the best polymer fibers for strengthening engineering cement composites (ECCs). Therefore, PVA fiber can be utilized to create rubber concrete that has high tensile strength and strain capacity [14].

However, experimental research makes up the majority of the current study on the mechanical characteristics of rubber concrete materials. Finite element technology can be used to conduct computer meso-numerical simulation testing since the test settings are constrained and the test results are generally discrete. Time can be saved, and expenses can be decreased, in this way. Parameter analysis can be performed concurrently using the appropriate mathematical model, and the best approach can be chosen to fulfill the intended goal. Additionally, depending on prior experiments, it can forecast and analyze unsolved issues as well as preliminarily support the new theory. Rubber concrete reinforced with PVA fibers serves as the study's research object. The three-dimensional meso-mechanical analysis of PVA rubber/concrete under uniaxial compression was performed based on the random aggregate model in an effort to use a simple constitutive relation to reflect the intricate mechanical properties of rubber concrete on a macro level, solve the design calculation issue for PVA rubber/concrete materials, and provide a technical foundation for the creation and use of new building materials [15–18].

In this study, concrete was tested using a standard uniaxial compression full curve method using PVA fiber and rubber particles of varying composition, and the mechanical characteristics of the PVA rubber/concrete mixture were thoroughly examined. The PVA rubber/concrete is then viewed as a six-phase composite made up of the aggregate phase, mortar matrix, PVA fiber, rubber particles, aggregate–mortar interface, and rubber–mortar interface based on the mesoscale. To simulate the entire process of PVA rubber/concrete with varying dosages from integrity to damage and cracking, a mesoscale numerical model of PVA rubber/concrete was constructed. In order to confirm that the mesomodel is accurate, the simulation results and experimental findings are compared at the end. This work presents a theoretical foundation for the structural analysis and design of PVA rubber/concrete in addition to demonstrating that PVA fiber may be employed as a novel way to improve the mechanical properties and durability of rubber concrete. The technology research roadmap is shown in Figure 1.

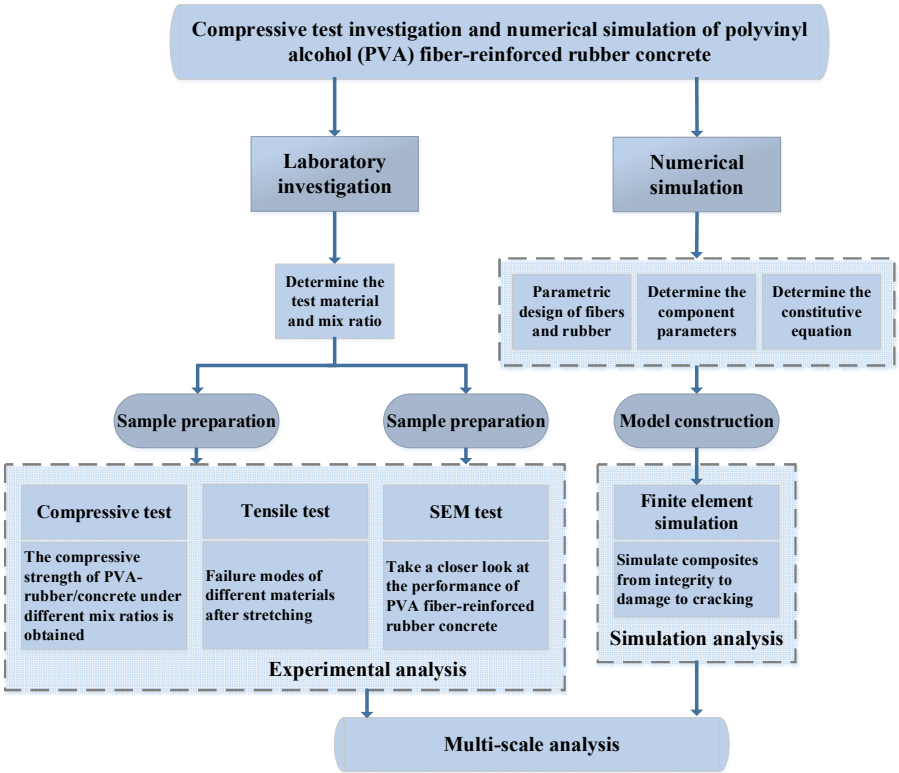

Figure 1. Technology roadmap.

2. Test Overview

2.1. Test Materials

The type of cement is regular Portland cement, P.O42.5. Tables 1 and 2 display the chemical make-up and physical characteristics. The coarse aggregate is continuously grading, with a particle size of 5~25 mm, an apparent density of 2703 kg/m^3, and a bulk density of 1550 kg/m^3. The fine aggregate is medium sand, with a fineness modulus of 5~25, an apparent density of 2650 kg/m^3, and a bulk density of 1850 kg/m^3. The particle size of rubber is 1~3 mm, and the basic properties are shown in Table 3. The polyvinyl alcohol (PVA) fiber is adopted, and the basic performance indices are shown in Table 4.

Table 1. Chemical composition of cement.

Composition	CaO	SiO_2	Al_2O_3	Fe_2O_3	MgO	SO_3	Other
Content/%	63.11	22.60	5.03	4.38	1.46	2.24	0.21

Table 2. Physical and mechanical properties of cement.

Specific Surface Area/(m^2 kg^{-1})	Standard Consistency/%	Coagulation Time/min		Flexural Strength/MPa		Compressive Strength/MPa	
		Initial Setting Time	Final Setting Time	3 d	28 d	3 d	28 d
370	27	150	205	4.8	8.0	29.2	49

Table 3. Basic performance indicators of rubber particles.

Particle Size Range /mm	Apparent Density /kg/m^3	Bulk Density /kg/m^3	Elastic Modulus /GPa	Poisson Ratio
1~3	1.03	610	0.07	0.449

Table 4. Basic performance index of PVA fiber.

Density /kg/m^3	Diameter /μm	Elastic Modulus /GPa	Length /mm	Tensile Strength/MPa	Break Elongation/%	Poisson Ratio
1.3	15	39	6	1704	12	0.3

The rubber particles are first soaked in an alkali solution [19] and then washed with tap water until the PH value of the rubber particles reaches neutral. After air drying, the rubber particles are added to the concrete mixture by replacing the fine aggregate with equal volume. The bonding force between PVA fiber and cement mortar under alkaline conditions is also very strong, and the fiber in the cement matrix tends to break rather than pull out when it is damaged by force [13]. PVA fiber uses the post-blending technique to ensure the fiber's dispersion, hydrophilicity, and interfacial performance with the matrix material.

We put the weighed cement, coarse aggregate, fine aggregate, rubber particles, and some water into the cement mortar mixer and then slowly added the prepared PVA fiber while stirring to ensure the uniformity of each component of the mortar. After mixing, we put the mortar into the greased mold and then placed it on the vibration table to vibrate for one minute. The formwork was removed after one day and cured for 28 days under standard conditions (20 $\pm$ 2 °C, humidity $\geq$ 95%).

2.2. Test Mix Proportion

Refer to JGJ55-2011 *Specification for Mix Proportion Design of Ordinary Concrete* to determine the concrete mix proportion. The two key research considerations in the creation of specimens are PVA content and rubber content. The water–cement ratio for plain concrete (PC) specimens is 0.4, and they are created in accordance with the strength grade C30. The fine aggregate is replaced by an equal volume of rubber particles to add the rubber particles at replacement rates of 0%, 10%, 20%, and 30%, respectively. PVA doping accounts for 0%, 0.5%, 1.0%, and 1.5 % of the volume, respectively. The particular mix proportion is presented in Table 5 and is developed for the 13 groups of PVA-fiber-reinforced rubber concrete. The specimen size was 100 mm× 100 mm× 100 mm, and there were 6 repeated specimens in each group. The mean value of mechanical strength and corresponding error bars for 7 and 28 days were calculated respectively, and the arithmetic mean value of measured values of 3 specimens was used as the compressive strength value of reconstructed specimens. After 28 days of curing in the standard curing room, the uniaxial compression stress–strain full curve test was carried out.

Table 5. PVA rubber/concrete mix ratio.

Name	Cement/ kg/m^3	Water /kg/m^3	Fine Aggregate /kg/m^3	Coarse Aggregate /kg/m^3	Rubber Particles /kg/m^3	PVA Fiber /kg/m^3
PC	400	160	799	1106		
RC10%	400	160	719	1106	32.6	
RC20%	400	160	639	1106	65.4	
RC30%	400	160	559	1106	97.7	
RC10%-PVA0.5%	400	160	719	1106	32.6	19.4
RC10%-PVA1.0%	400	160	719	1106	32.6	38.6
RC10%-PVA1.5%	400	160	719	1106	32.6	57.8
RC20%-PVA0.5%	400	160	639	1106	65.4	19.4
RC20%-PVA1.0%	400	160	639	1106	65.4	38.6
RC20%-PVA1.5%	400	160	639	1106	65.4	57.8
RC30%-PVA0.5%	400	160	559	1106	97.7	19.4
RC30%-PVA1.0%	400	160	559	1106	97.7	38.6
RC30%-PVA1.5%	400	160	559	1106	97.7	57.8

Notes: PC—Plain concrete; RC—Rubber particles; PVA—PVA fiber; RC10%, RC20%, RC30%—Rubber volume substitution ratios of 10%, 20%, and 30%, respectively; PVA0.5%, PVA1.0%, PVA1.5%—PVA fiber volume fractions of 0.5 vol%, 1.0 vol%, and 1.5 vol%, respectively.

2.3. Loading Device and Test Method

The method in the reference of the uniaxial compressive stress–strain full curve test of concrete was carried out [20]. Y250 digital display electric stress direct shear equipment was used for loading, and the TYE-2000E testing machine was used for tensile testing. The Y250 digital display electric stress direct shear equipment is able to directly measure and record the stress–strain curve during the test. Before the official start of the test, preloading was carried out to eliminate the gap between the specimen and the equipment, and the preloading load was equivalent to 40% of the failure load. The test methods were carried out in accordance with the Standard for Test Methods for Mechanical Properties of Ordinary Concrete (GB/T50081-2002). The loading rate of the testing machine is 0.5 MPa/s; when the specimen is close to failure and begins to deform sharply, the testing machine stops loading and records the failure load. Due to the use of non-standard specimens, the compressive strength reduction coefficient is 0.95, and the splitting tensile strength reduction coefficient is 0.85. Figure 2 shows the specimen test device.

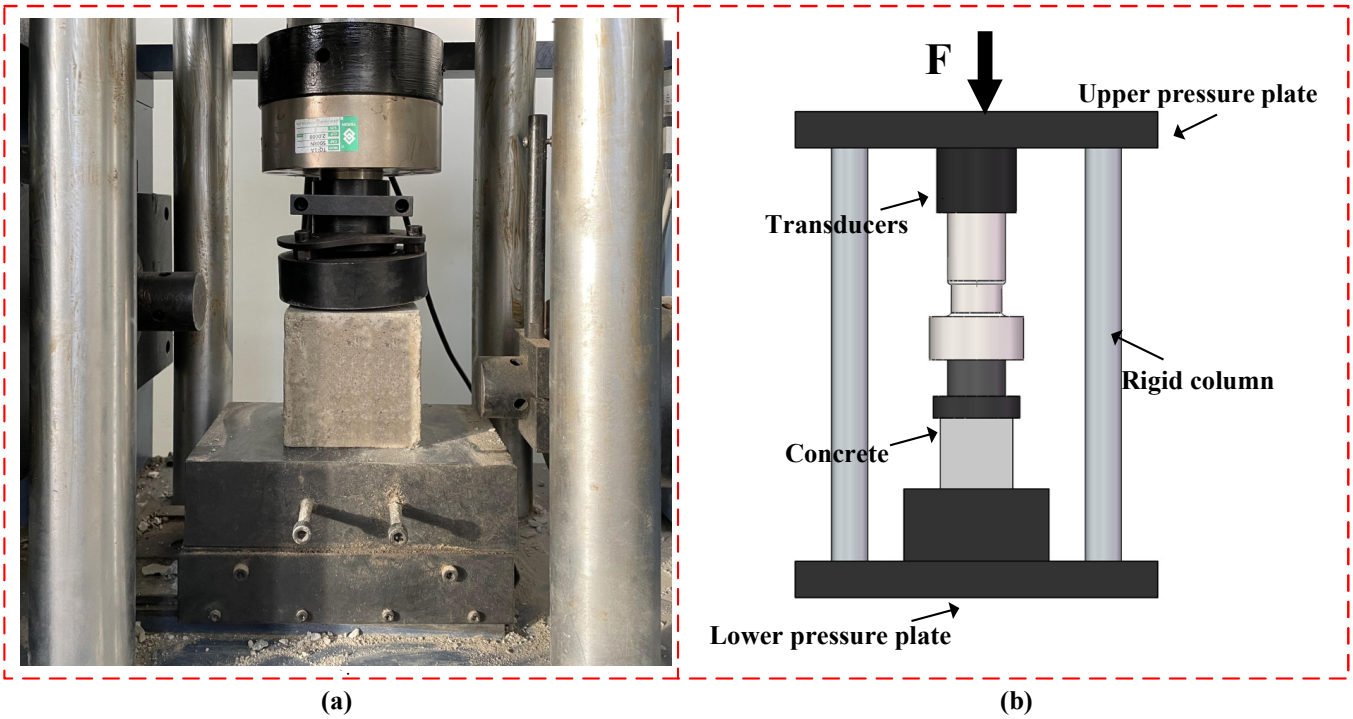

Figure 2. Specimen test device: (**a**) Setting of test; (**b**) Testing apparatus.

3. Test Process and Failure Mode

3.1. PVA Rubber/Concrete Failure Process and Morphology

At the initial stage of compression of the PVA rubber/concrete specimen, elastic deformation occurs in the mortar matrix and rubber particles, and there is no initial crack development. At the beginning of the crack, the rubber particles play a certain role in preventing the crack in the mortar matrix, while PVA plays a limited role at this time. When the rubber particles are introduced, the bubbles around them will increase. The weak zone of the specimen is mainly located at the interfacial connection between the mortar matrix and the rubber particles. When the pressure reaches a certain value, the interfacial connection between the two will be damaged first. The pressure will gradually increase, the cracks will gradually expand, the lateral deformation will increase, and obvious short cracks will appear on the surface. At this time, PVA also plays a role in preventing cracks because of the crack expansion. PVA effectively stops the crack development rate. The lateral deformation of the specimen is restrained. When the fracture occurs, the macro cracks extend and expand, forming the main cracks and distributing parallel to the diagonal. The specimen continues to be damaged, the crack further expands, the main crack runs through and continues to grow, the concrete around the crack peels off, and PVA is pulled out slowly. However, because of the PVA fiber bridging effect, the cracked section can still be closely connected. In the convergence stage, the crack forms a failure zone, PVA is pulled out, and the load between cracks is mainly borne by PVA. With the reduction in PVA, the specimen is finally destroyed.

This is shown in Figure 3. When the PC specimen is damaged, the crack is split along the height direction of the specimen, the crack width is large, the specimen is seriously broken, the stress drops sharply after the peak value, and the brittle failure characteristics are obvious. In the whole compression failure stage of rubber concrete, the rubber particles absorb part of the energy due to their own elasticity during the stress deformation and act as dampers in the mortar matrix, slowing down the generation and development of internal cracks in the specimen and reducing the brittleness of the specimen, but their bearing capacity is insufficient in the later stage of failure. The addition of PVA enhanced the later bearing capacity of rubber concrete and cooperated with rubber to participate

in the transverse crack stress, making the cracks more compact, slowing down the crack growth rate of the specimen, and enhancing the ductility of the specimen.

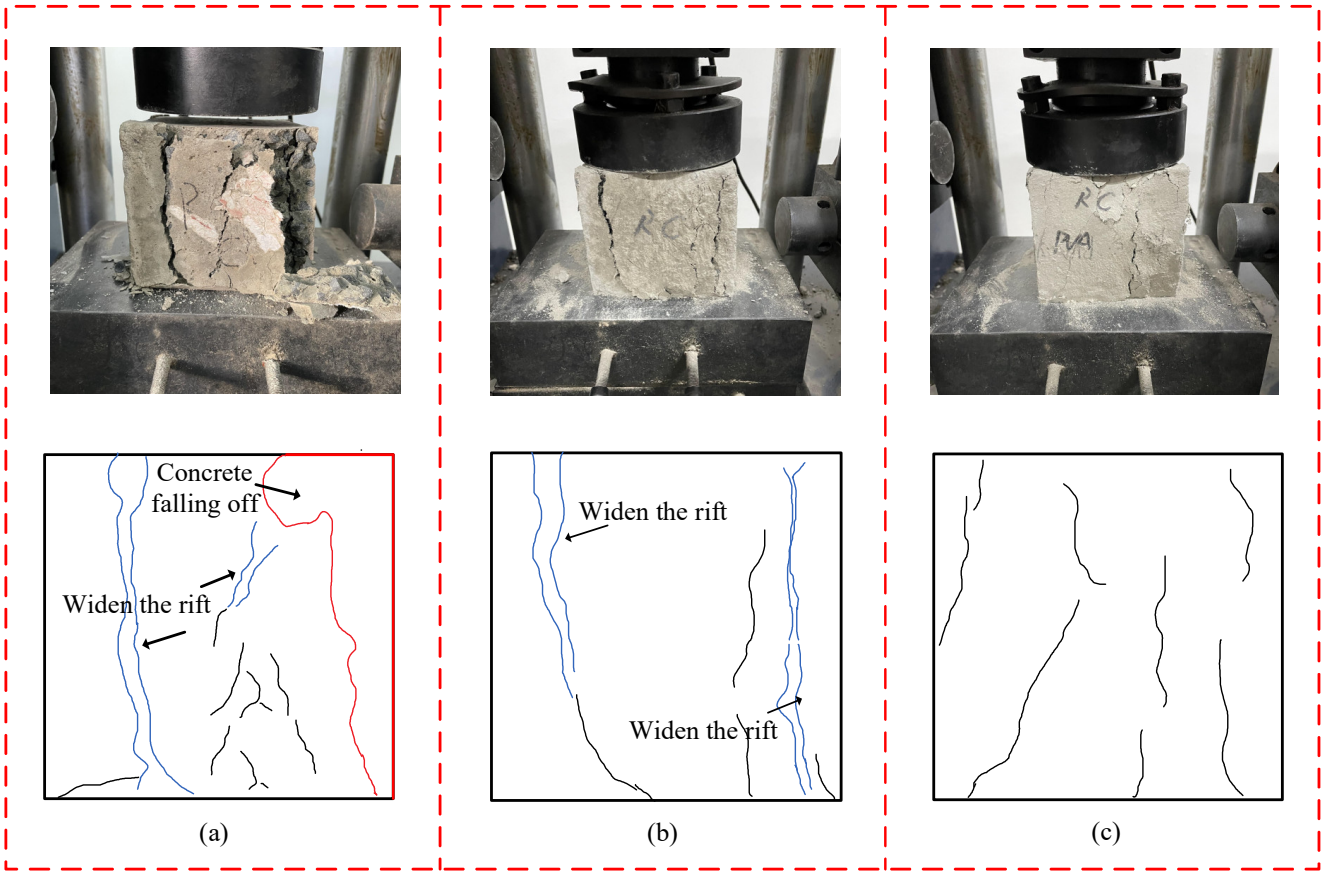

Figure 3. Compressive failure modes of concrete with different compositions: (**a**) Plain concrete; (**b**) Rubber concrete; (**c**) PVA rubber/concrete.

The failure characteristics of specimens with different ages and different mix ratios are similar; they are single inclined plane shear failure or tensile failure, like the ultimate failure morphology of specimens in Figure 3. The inclination angle of the inclined plane is close to vertical. The internal factor may be the more uniform stress distribution within the specimen, which also contributes to the uniformity of the radial strain at various axial points and lessens the impact of the end effect. In the cubic compression test, the specimen without elastic material, as shown in Figure 4a, undergoes compression deformation and transverse elongation deformation during the compression process. In the initial stage of loading, microcracks appear on the concrete surface and gradually develop into edges and corners. With the increase in the load, the microcracks develop rapidly, the specimen's internal and surface expansion occurs, and the specimen's surface falls off seriously. Finally, the concrete is crushed, and the failure pattern appears wedge-shaped on the surface of the specimen, which is understandable for brittle failure. In the process of compression failure, cracks appear later in the specimens mixed with elastic materials than in those without, as shown in Figure 4b–d. In the early stage, the cracks obviously become smaller, and in the later stage, the microcracks gradually develop and become larger, and the surface spalling of the specimen is reduced. Until the end of loading the PVA rubber/concrete specimens, the specimens do not undergo wedge failure and maintain good integrity, showing significant plastic failure. PVA has a positive impact on integrity by reducing cracking and shedding.

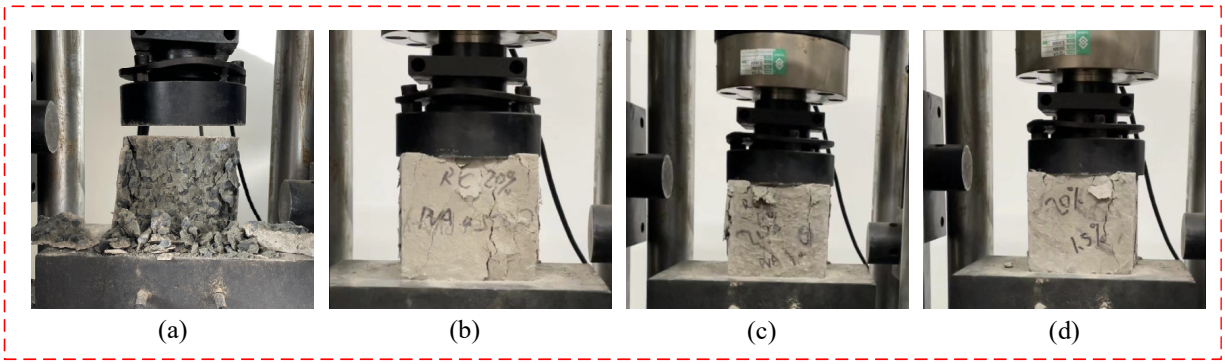

Figure 4. Failure modes in cubic compressive tests: (**a**) Plain concrete; (**b**) RC20%-PVA0.5%; (**c**) RC20%-PVA1.0%; (**d**) RC20%-PVA1.5%.

Figure 5 illustrates the typical failure mode of PVA rubber/concrete specimens in the splitting tensile test. In the test, as shown in Figure 5a, the specimen of the inelastic material starts to show microcracks along the gasket when the load increases for the first time. When the ultimate splitting strength is reached, the crack quickly penetrates the bottom and top surfaces of the specimen. At this point, the load suddenly decreases, the specimen splits into two parts, and obvious ringtones can be heard when damaged, which indicates a brittle failure. The specimen's failure surface reveals that the fracture primarily happens where the aggregate and cement mortar meet, with the aggregate itself not being pushed off. Figure 5b demonstrates how the specimen's brittle failure mode changed following the addition of elastic material rubber; now, there is no discernible ringing during damage, the failure mode is a plastic failure, and the fracture narrows. As the load increases, the surface fissures in the concrete gradually widen, pieces of the concrete start to crumble, and cracks appear through the bottom and top surfaces. Figure 5c illustrates that the specimen did not split into two pieces because of the fiber connection between the fissures. The outcomes demonstrate that the inclusion of rubber can successfully prevent the development of cracks. PVA uses a significant amount of energy, and fissures are primarily produced on the specimen's surface during the destruction process. Concrete spalling and fragmentation are not serious phenomena, but they become more noticeable as PVA content rises.

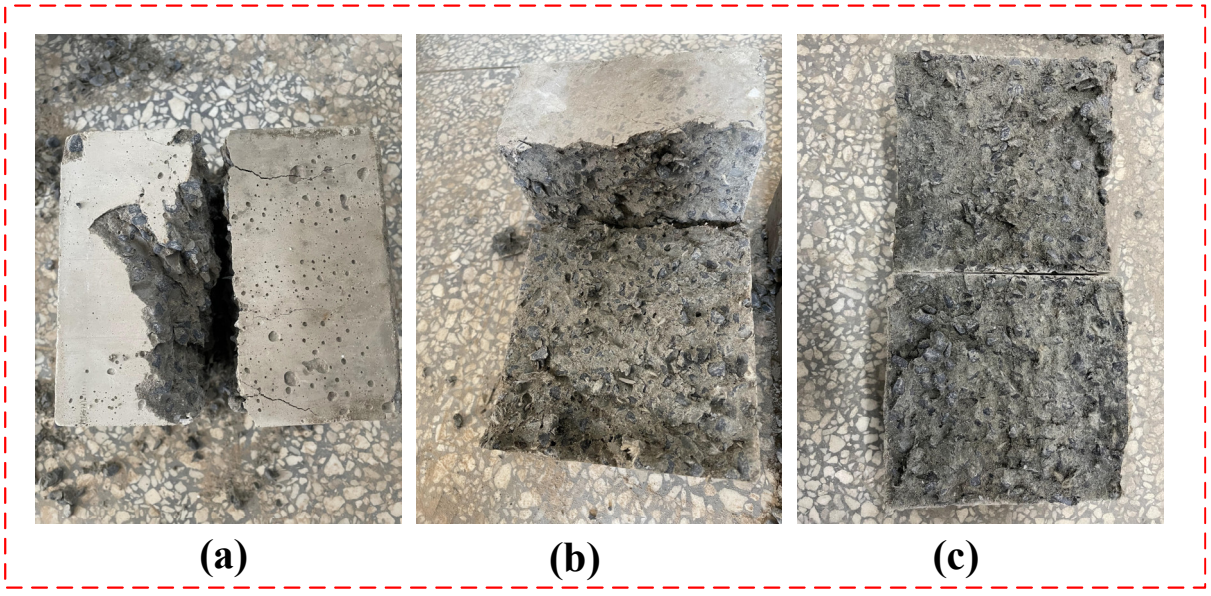

Figure 5. Failure modes in splitting tensile tests: (**a**) Plain concrete; (**b**) Rubber concrete; (**c**) PVA rubber/concrete.

3.2. PVA-Rubber/Concrete Compressive Stress Strain

Figure 6 depicts the uniaxial compression-induced failure process of PVA rubber/concrete specimens with various contents. The side faces of the specimens are nearly parallel to the compression loading direction under various PVA and rubber replacement rates, and the failure forms of the specimens with various dosages are similar. Conversely, the cracks of rubber concrete reinforced with PVA are denser, and the compressive strength is also improved to varying degrees. The investigation reveals that rubber belongs to the hydrophobic material family, whereas cement mortar is hydrophilic. As a result, there is poor compatibility and interfacial bonding ability when rubber and cement mortar are combined. The comparison of experimental failure forms demonstrates that when PVA is not added, the concrete crumbles and develops huge fissures. The number and width of concrete cracks are reduced after the addition of PVA, and the compressive strength is also enhanced to varying degrees.

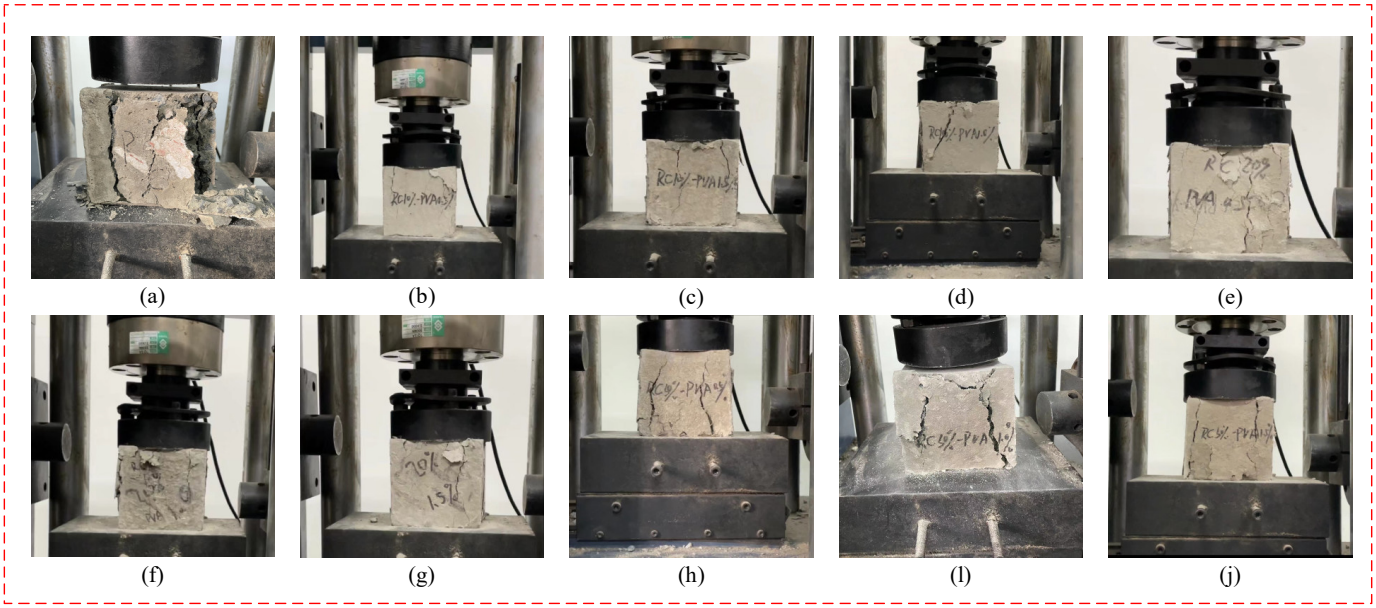

Figure 6. Compression failure morphology of PVA rubber/concrete specimens with different contents: (**a**) PC; (**b**) RC10%-PVA0.5%; (**c**) RC10%-PVA1.0%; (**d**) RC10%-PVA1.5%; (**e**) RC20%-PVA0.5%; (**f**) RC20%-PVA1.0%; (**g**) RC20%-PVA1.5%; (**h**) RC30%-PVA0.5%; (**i**) RC30%-PVA1.0%; (**j**) RC30%-PVA1.5%.

The compressive strength of specimens with different material substitution rates is shown in Figure 7. PC pressure is 27.45 MPa; the pressure of RC10% is 19.87 MPa, and the compressive strength of PVA is 20.35 MPa, 20.97 MPa, and 20.15 MPa when the replacement ratio of RC10% is 0.5%, 1.0%, and 1.5% respectively. The pressure of RC20% is 16.56 MPa, and the compressive strength of PVA is 16.95 MPa, 17.39 MPa, and 16.87 MPa when the replacement ratio of RC20% is 0.5%, 1.0%, and 1.5% respectively. The pressure of RC30% is 12.95 MPa, and the compressive strength of PVA is 13.25 MPa, 13.61 MPa, and 13.21 MPa when the replacement ratio of RC30% is 0.5%, 1.0%, and 1.5% respectively. After calculation, when the replacement ratio of rubber content is 10%, 20%, and 30%, respectively, the compressive strength of RC is 27.61%, 39.67%, and 52.82% lower than that of PC. When the PVA substitution rate is 0.5%, 1.0%, and 1.5%, respectively, the compressive strength increased by 2.36%, 5.24%, 1.38%, 2.30%, 4.77%, 1.83%, 2.26%, 4.84%, and 1.96% compared with RC10%, RC20%, and RC30%, respectively. The analysis of these characteristic values concludes that the rubber substitution rate increases and the uniaxial compressive strength of the specimen decreases. The addition of PVA enhanced

the compressive strength of rubber concrete to varying degrees, and the enhancement effect of 1.0% PVA was the most significant.

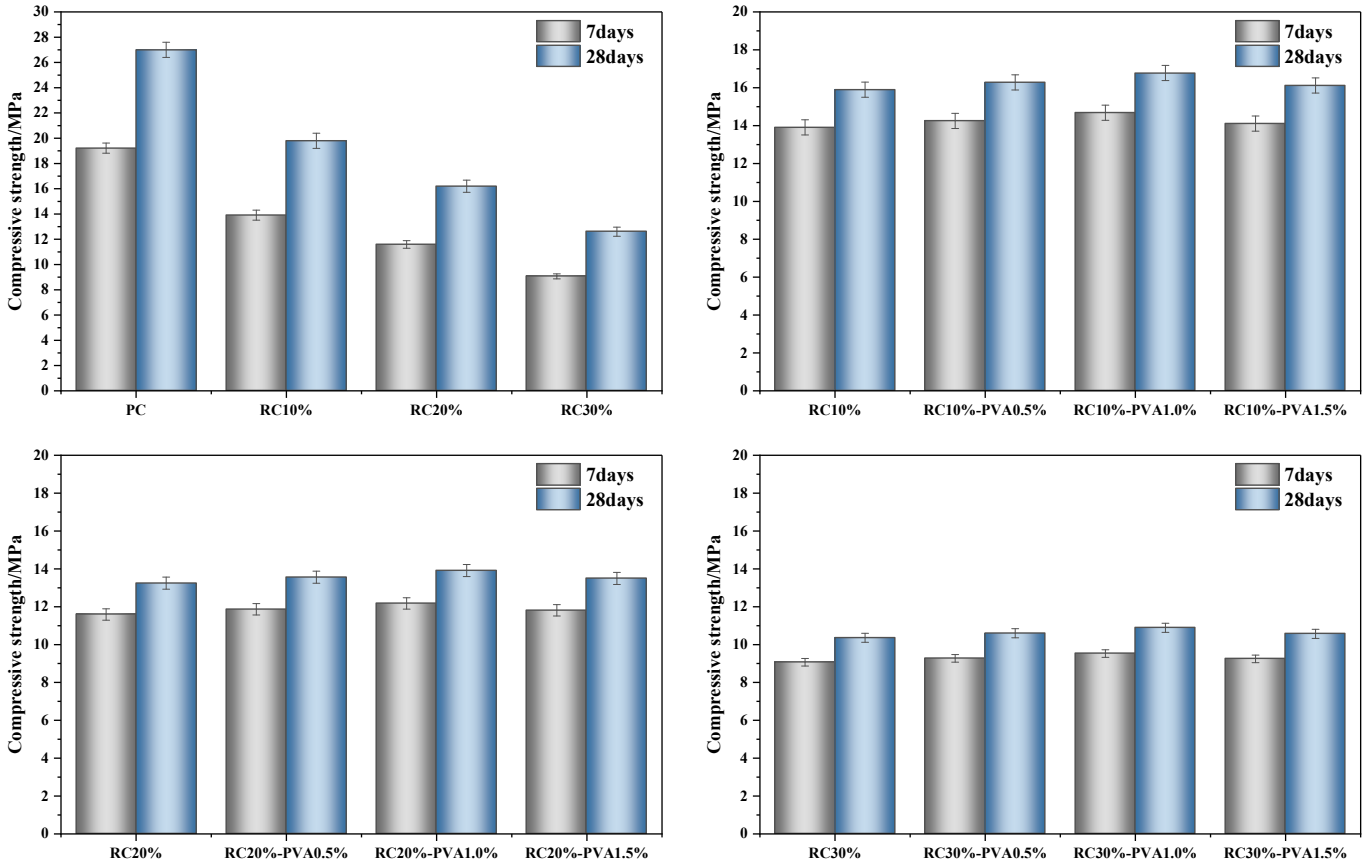

Figure 7. Compressive strength of specimens with different material substitution rates.

Under uniaxial compression, Figure 8 depicts the entire stress–strain curve of the PVA rubber/concrete specimen. As can be seen from Figure 8, with the increase in rubber content, the corresponding peak stress ductility of rubber/concrete increases, but the peak stress decreases. The reason is that the interface zone of the rubber and the cement matrix is weak due to their poor compatibility. For PVA rubber/concrete, when the rubber content is unchanged, the peak stress and strain of the corresponding peak stress increase with the increase in PVA content. However, on the contrary, when the content of PVA is excessive, the peak stress of the corresponding peak stress decreases, because of the agglomeration phenomenon of PVA, as shown in Figure 9d. When the stress on the matrix increases, the microcrack propagation in the region with low PVA content will not be hindered; thus, the overall performance of the matrix decreases. As a result, adding the proper amount of PVA to rubber/concrete can improve its bearing capacity, fracture width, and expansion rate.

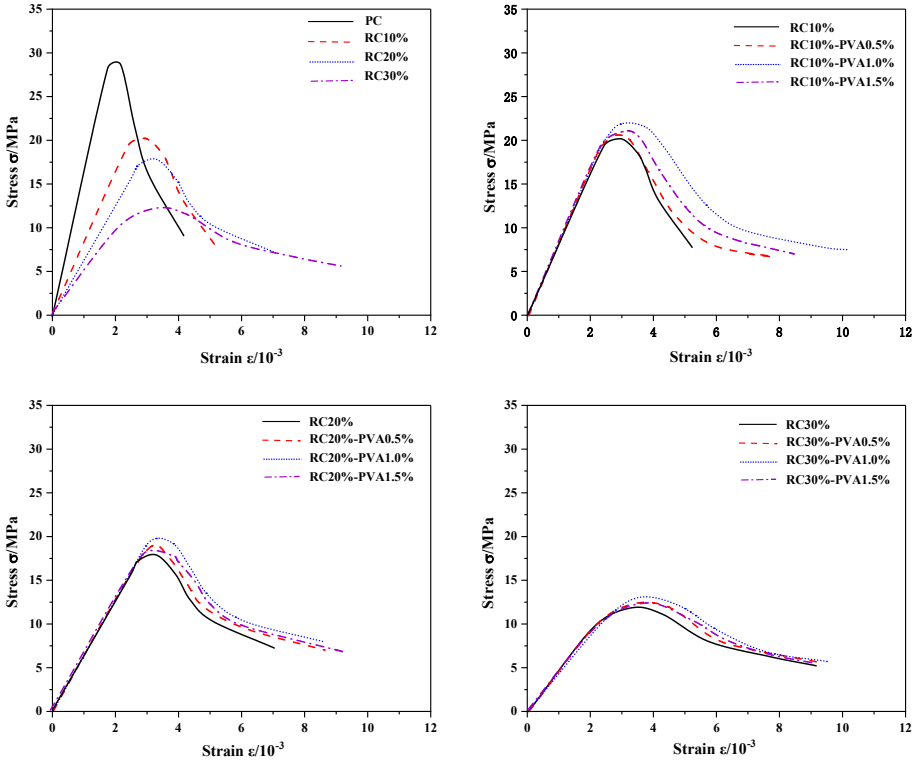

Figure 8. Full stress–strain curve of PVA rubber/concrete specimen under uniaxial compression.

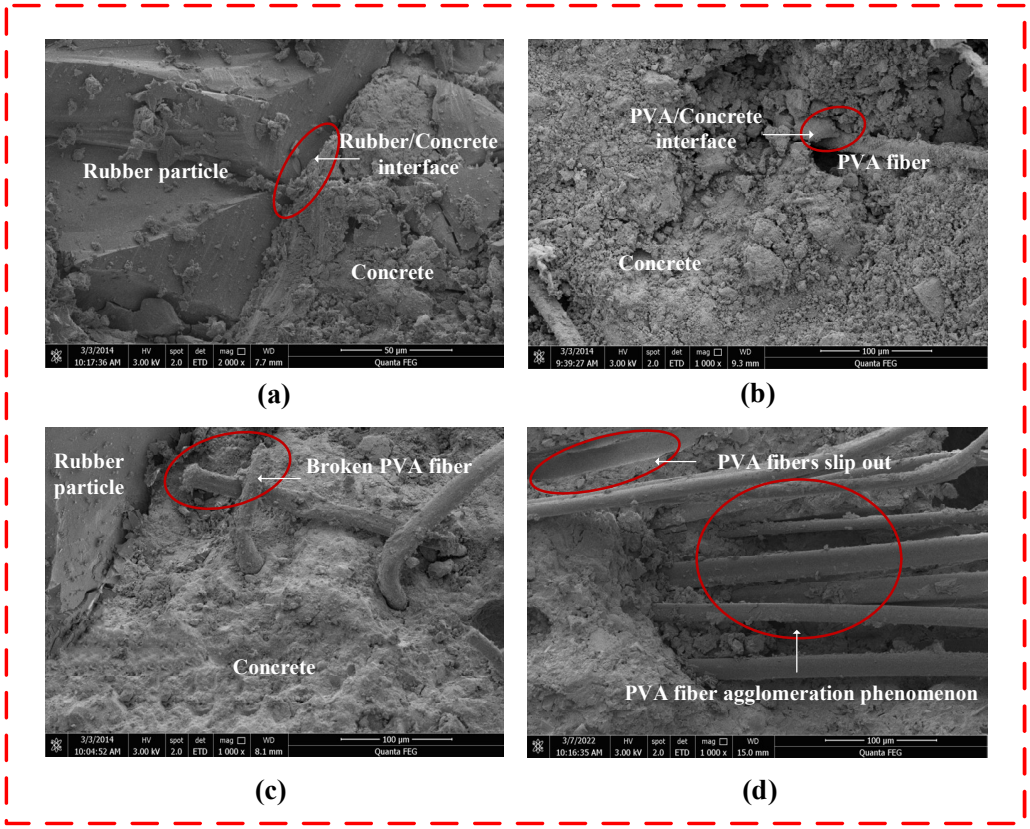

Figure 9. Micromorphology of the specimen: (**a**) Rubber concrete; (**b**) PVA rubber/concrete; (**c**) PVA destruction form; (**d**) PVA aggregation phenomenon.

3.3. Failure Mechanism of PVA Fiber Pull-Out Rubber Concrete Interface

Figure 9a demonstrates that the interfacial area between rubber and the cement matrix is relatively weak because rubber is an organic material with poor compatibility. As the content of rubber increases, more bubbles will be introduced into the RC mixture, increasing the internal pores of the concrete and decreasing the compressive strength of the RC. Figure 9b illustrates how greater shedding occurs on the fracture surface when the PVA-fiber-reinforced concrete matrix is disturbed. However, the addition of PVA fiber to the rubber concrete eliminates the brittleness of plain concrete, and the bonding force between PVA and cement mortar is also very strong under alkaline conditions. In the late stage of PVA rubber/concrete specimen failure, three-dimensional reinforcement is provided for the structure to resist internal tension, and the failure rate of the specimen is restrained. As shown in Figure 9c, the fiber tends to break rather than pull out when it is stressed [13]. As a result, the strength of rubber concrete is improved. Even after the crack penetrates the whole structure, the failed parts will gather together because of the fiber bridging effect. However, if there is an excessive amount of PVA present, the fibers will aggregate, as seen in Figure 9d, and aggregated fibers will create a new type of complex. The fibers in this area are prone to slipping and deforming and are unable to support the weight. Additionally, the remaining cement matrix's fiber content is decreased. If the matrix's tensile stress is raised, the matrix's ability to expand into microcracks will not be hampered, which lowers the matrix's overall effectiveness.

4. Numerical Analysis

4.1. 3D Geometry Model Creation

Based on the meso simulation research carried out by Masad et al. [21], it is found that concrete is usually regarded as a three-phase composite (aggregate phase, mortar matrix phase, and interfacial phase), so the PVA rubber/concrete specimen studied in this paper is regarded as a six-phase composite composed of aggregate phase, mortar matrix, PVA fiber, rubber particles, aggregate–mortar interface, and rubber–mortar interface, as shown in Figure 10b. Due to the small size of the interfacial structure, it is not easy to obtain it directly from the test. Considering that the properties of the interface layer are similar to those of the mortar interfacial layer but the strength has decreased to varying degrees, the material parameters of the interfacial layer can be reduced in a certain proportion according to the material parameters of the mortar matrix. The thickness of the aggregate–mortar interface is 0.5 mm [22–24], the thickness of the rubber–mortar interface is 0.2 mm, and the diameter of PVA fiber is too small. Therefore, the interface between fiber and mortar is preset to 0 thickness.

The concrete aggregate is graded as Grade II, and the aggregate size range is 5~25 mm. According to the three-dimensional concrete grading formula proposed by Fuller [25], we can determine the distribution volume at all levels, as shown in the following formula:

$$P = 100\sqrt{\frac{D_0}{D_{max}}} \tag{1}$$

In the formula, P is the percentage of aggregate passing through the D_0 sieve hole with a certain diameter, D_0 is the diameter of the sieve hole, and D_{max} is the maximum aggregate particle size. To simplify the calculation, these coarse aggregates are equivalent to spheres with two particle sizes [26], namely, aggregate particles with a particle size of 20 mm and 15 mm. The 3D geometry model is shown in Figure 10.

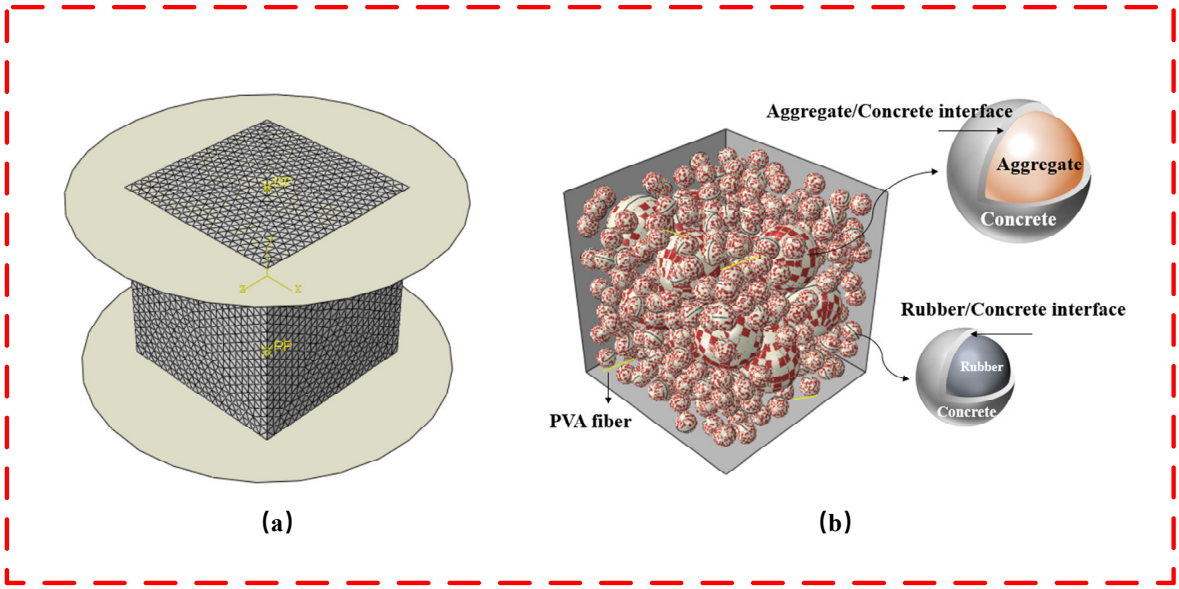

Figure 10. Uniaxial compression 3D mesoscopic model: (**a**) Uniaxial Compression Model; (**b**) 3D Aggregate Spatial Distribution.

In order to achieve the rapid establishment of the composite model and improve the efficiency of the composite analysis based on finite element calculation, this paper, based on the micromechanics of finite element calculation, compiles a Python script to generate points that are uniformly distributed over time in the designated area and then generate fiber elements in any direction over time from these points. The uniform distribution function in the NumPy function library is used to simulate the random release process of rubber particles. Finally, the properties of fiber and particle materials, which are different from those of mortar, are assigned in batches, and the interfacial transition zone [27–32] is generated. The creation of six-phase composite materials is completed, and the uniaxial compression damage form is simulated based on the global insertion of cohesive elements. The three-dimensional mesh model under different dosages is shown in Figure 11. We believe that our finite element modeling method improves the traditional modeling method, which is not only more accurate but also more reliable in the simulation results.

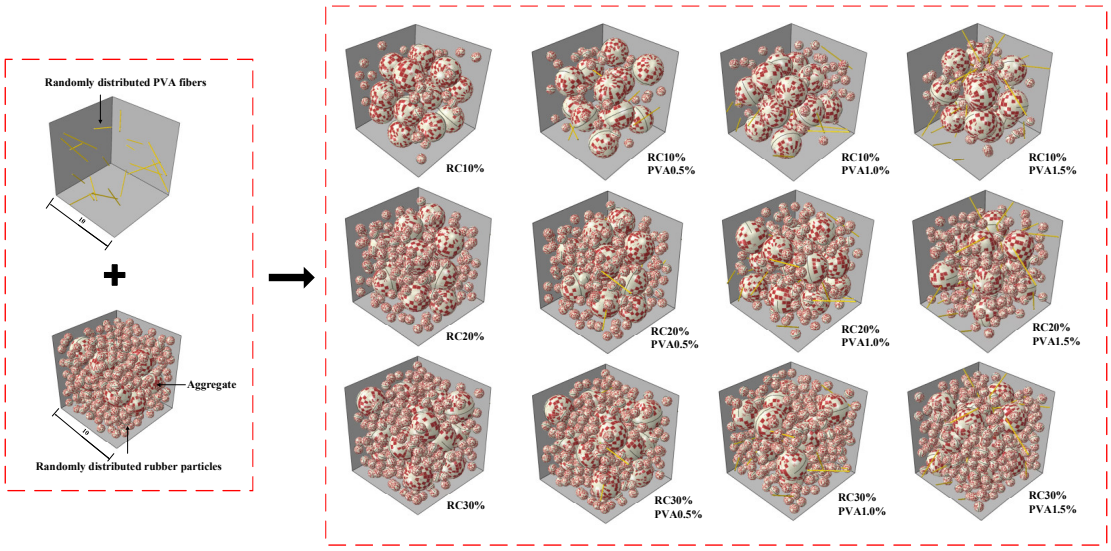

Figure 11. Three-dimensional mesomodel with different dosages.

4.2. Material Constitutive Model

The research of domestic and foreign scholars on the PC constitutive model has been relatively mature, such as the Carreira Chu model [33], the Guo Zhenhai model, and the damage constitutive model in GB50010-2010. The constitutive models used in the experimental research on rubber/concrete are mostly modified based on different constitutive models of PC [34,35], and the test results obtained according to different rubber particle content, particle size, reference concrete strength, and other factors are different from the corresponding constitutive models. At present, there is no special constitutive model to simulate the mechanical properties of PVA rubber/concrete. Concerning previous work [21], the plastic damage material model in Abaqus material library is used for the PVA rubber/concrete matrix studied in this finite element analysis, which can simulate well the failure mode of concrete under compression and is also used in numerical models by many scholars [24,36]. Refer to the model proposed by Popovics et al. [37] for the matrix compression stress–strain relationship under uniaxial load, as shown in Figure 12a. The calculation formula is as follows:

$$\sigma_c = \frac{f_c \lambda (\varepsilon_c / \varepsilon_0)}{\lambda - 1 + (\varepsilon_c / \varepsilon_0)^{\lambda d}}, \tag{2}$$

$$\lambda = \frac{E_0}{E_c - (f_c / \varepsilon_0)}, \tag{3}$$

$$d = \begin{cases} 1, \varepsilon_c / \varepsilon_0 \le 1 \\ 0.67 + \frac{f_c}{62} \ge 1, \varepsilon_c / \varepsilon_0 > 1' \end{cases} \tag{4}$$

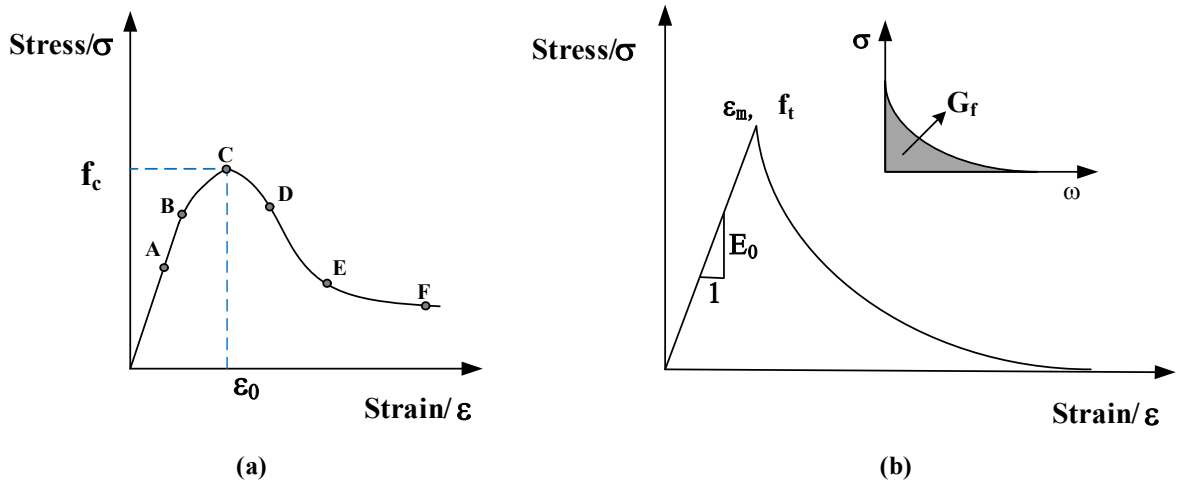

Figure 12. Uniaxial stress–strain curves for PVA rubber/concrete: (**a**) Uniaxial compressive stress–strain curves for PVA rubber/concrete; (**b**) Uniaxial stretch stress–strain curves for PVA rubber/concrete.

In the formula, σ_c is the concrete compressive stress; f_c is the compressive strength of ordinary concrete. In this paper, f_c = 30 MPa; ε_0 is the compressive strain of concrete corresponding to the f_c, and 0.002 is taken in this paper; the elastic modulus E_c is calculated according to the US ACI specification:

$$E_c = 4730\sqrt{f_c}, \tag{5}$$

The tensile pressure strain curve of concrete is shown in Figure 12b, and the elastic modulus and compression initial tangent modulus E_0 is the same.

Fracture energy G_f is equal to the area enclosed by the stress crack width curve and the horizontal axis; the fracture energy G_f is calculated according to the European EC2 specification:

$$G_f = \alpha(0.1f_c)^{0.7}, \quad (6)$$

In the formula, the G_f unit is N/mm, the f_c unit is MPa, and the coefficient α is related to the maximum particle size D_{max} aggregate.

For other parameters of the concrete plastic damage model, the default values are adopted: the expansion angle is 32°, the eccentricity is 0.1, the ratio of biaxial and uniaxial compressive strength is 1.16, the K-factor is $\frac{2}{3}$, and the viscosity coefficient is 0.005.

In the meso-analysis, the material mechanical properties of the interfacial transition layer and the mortar matrix are similar, so the interfacial transition layer uses the same plastic damage constitutive model as the concrete matrix [36,38], but the strength of the interfacial transition layer will be reduced according to a certain proportion concerning the concrete matrix [39]. The main parameters are shown in Table 6.

Table 6. Parameters of concrete components used in finite element analysis.

Parameters	Elastic Modulus/(GPa)	Poisson Ratio	Compressive Strength/(MPa)	Tensile Strength/(MPa)
Aggregate phase	50	0.2	80	8
Mortar phase	30	0.2	49	3.9
Rubber particles	0.07	0.499	25	2.5
PVA fiber	39	0.3	/	1704
Aggregate/Mortar Interface	21.6	0.2	35.3	2.8
Rubber/Mortar Interface	6	0.2	1.0	15

The three-dimensional mesh model of the PVA rubber/concrete cube specimen under uniaxial compression established in this paper is shown in Figure 10a. The side length of the specimen is 100 mm. The boundary and loading conditions [26,40] set for uniaxial compression are as follows. Using displacement boundary conditions, displacement constraints are set at the bottom of the specimen to limit the displacement in X, Y, and Z directions. The lower boundary constraints are $U_X = 0$, $U_Y = 0$, and $U_Z = 0$. The load is at the top of the model; considering the lateral constraints of the loading end on the concrete, the load is loaded in the form of displacement, with a vertical load of $U_Y = -5$ mm. We set a rigid uniform loading plate structure above the specimen, with a thickness of 4 mm, and lay it evenly on the top of the simulated specimen. This operation effectively avoids the phenomenon of local stress concentration and does not affect the further implementation of displacement load when the top element is damaged by compression or tension, ensuring the integrity of the calculation process. Considering the influence of element size on the nominal strength and failure mode, the element size in the finite element analysis in this paper is divided into 1 mm [26].

4.3. Finite Element Analysis Results and Discussion

The mesomodel simulates the whole process of the concrete specimen from integrity to damage to cracking when it is damaged under uniaxial compression, as shown in Figure 13. It can be seen that the external failure modes of the specimens are basically similar, with some inclined cracks and local concrete peeling. From the distribution of the internal damage of concrete materials, the damage is mainly concentrated in the interfacial phase around the aggregate particles, which are also the areas with the thinnest and weakest mechanical properties of concrete materials. A lot of damage and cracks occur in the interfacial phase and then spread and evolve to other areas. Under the action of load, the internal damage cracks of concrete soon reach the failure state, and even some damage cracks have not yet expanded to the surface when the entire specimen has lost its

bearing capacity, indicating that concrete specimens have greater brittleness in uniaxial compression failure.

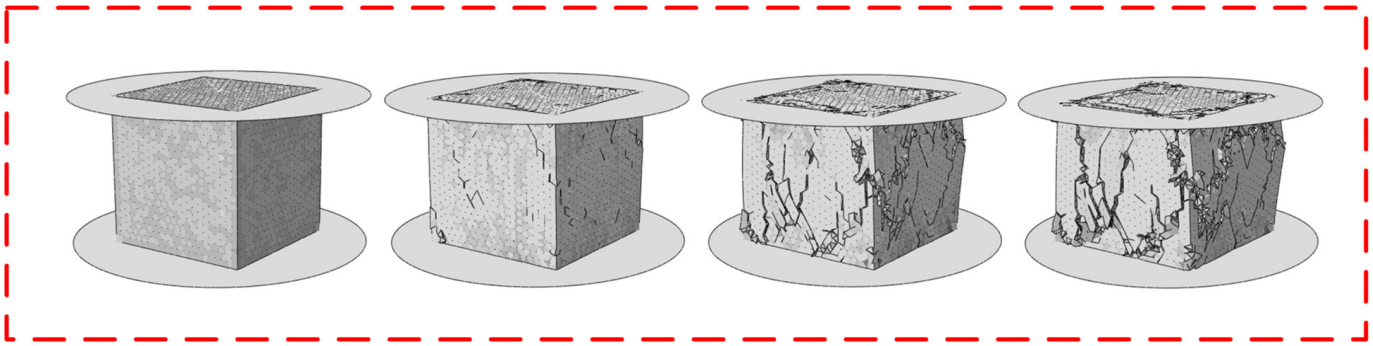

Figure 13. The whole process of the model from intact to damage to crack.

Although the data from mesoscale numerical simulation are not completely consistent with the macro test results, the overall trend is similar, which can characterize the uniaxial failure process of the specimen. In the mesoscale numerical simulation, with the increase in the load imposed on the plain concrete, the vertical compression deformation of the specimen occurs, and the horizontal direction extends to the four sides. The constraint effect of the upper and lower bearing plates makes the vertical deformation of the specimen small. There is no constraint in the middle of the specimen, so the horizontal deformation is the largest. The specimen gradually expanded outward from the middle, and with the further increase in pressure, the deformation of the specimen also increased until it finally failed, as shown in Figures 14 and 15. In the rubber concrete model, rubber is regarded as a kind of super elastic material, and the addition of rubber leads to the continuous change of rubber mortar interfacial structure. With the increase in rubber content, the number of rubber–mortar interfacial units, total interfacial units, and initial defect units increased, and the strength of rubber concrete showed a downward trend. The failure states of the PVA rubber/concrete model are divided into damaged and failed. Under a certain load, the elastic modulus of the model decreases gradually, but it still maintains certain mechanical properties, which is called damage. When the load continues to act, the model loses elasticity and its own mechanical properties, which is called failure. The PVA content will certainly improve the strength of rubber concrete. When the content exceeds a certain amount, the addition of PVA will reduce the adhesive force of the rubber concrete matrix and the strength value of rubber concrete, as shown in Figure 16, which is consistent with the conclusion reached by our test.

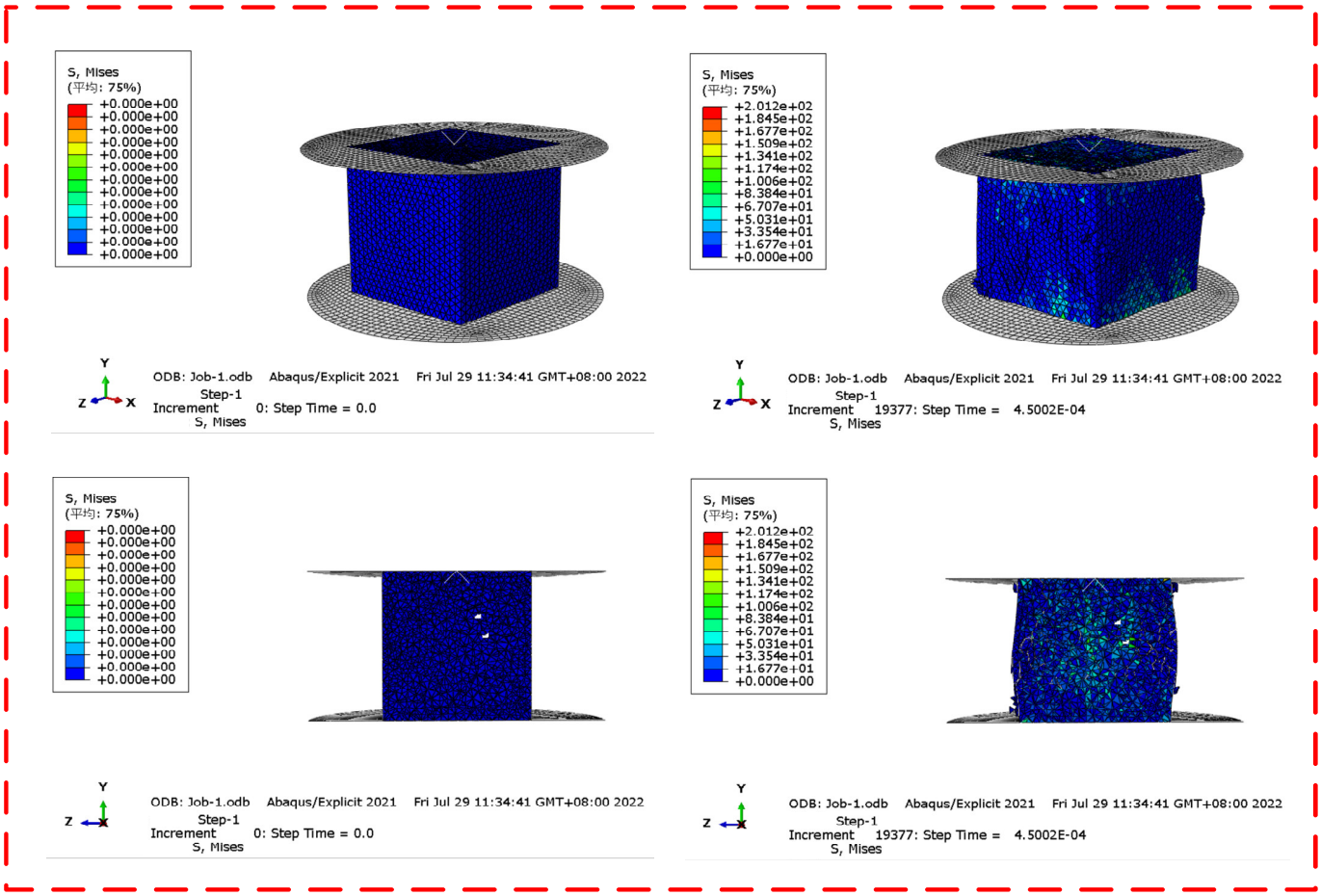

Figure 14. Stress damage cloud.

For a comparison of test and simulation findings, Figure 17 shows rubber concrete specimens with various contents and PVA specimens with various contents of 20% rubber. The figure shows that the stress–strain curves from the simulation and test are essentially consistent, demonstrating the good accuracy of the numerical simulation. However, the peak stress of the simulated stress–strain curve shifts a little bit more backward than that of the experimental stress–strain curve. This difference may be caused by the test's use of shear and friction forces, which could have an impact on the test's outcomes. Additionally, the constitutive relation used for numerical simulation is not the best one for this material, and a better relationship can be investigated later for simulation.

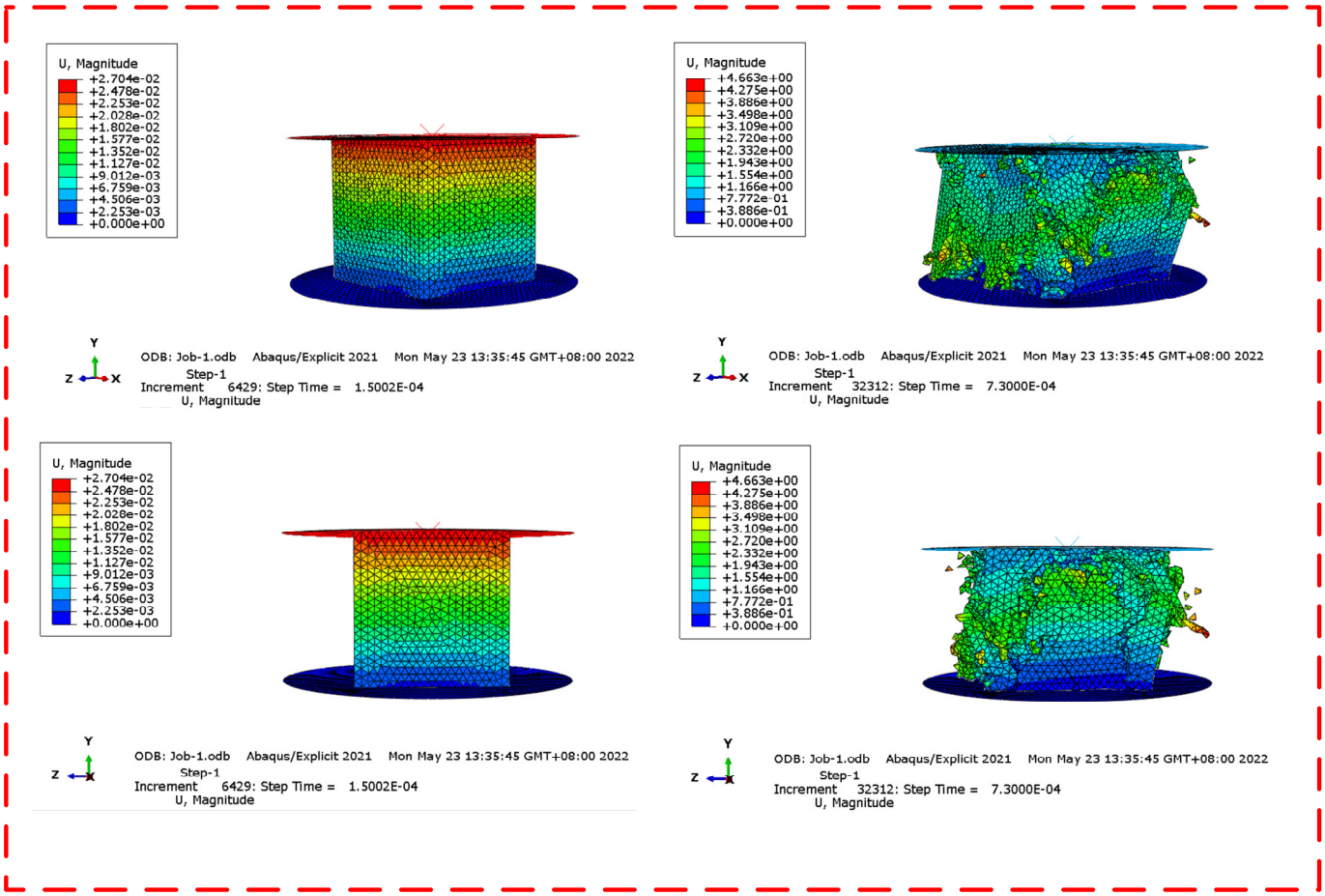

Figure 15. Displacement deformation cloud.

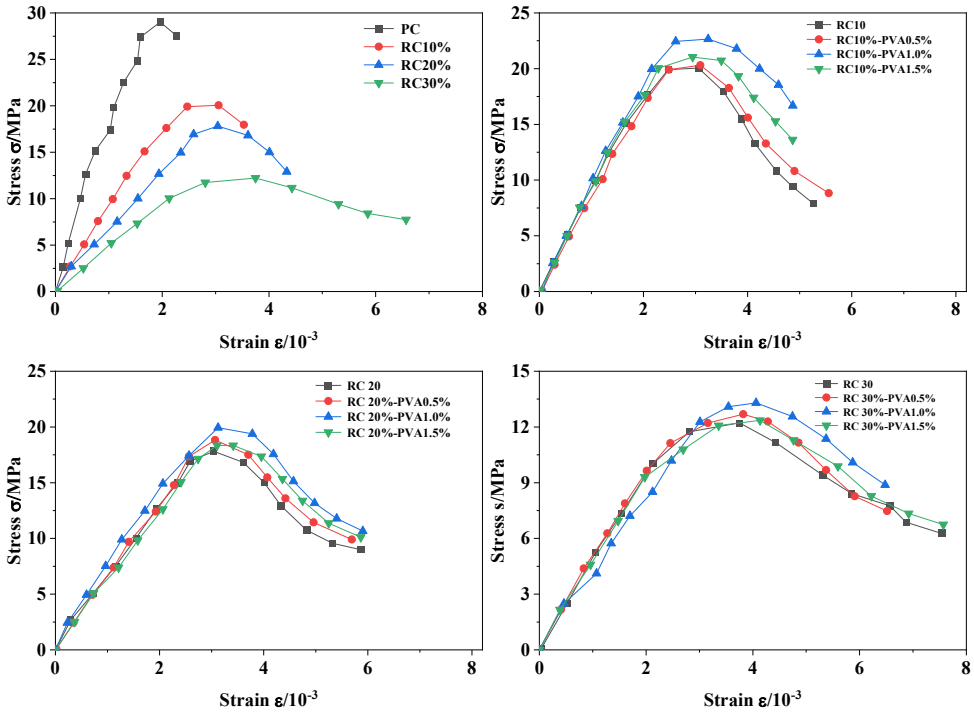

Figure 16. Finite element simulation of stress–strain curve.

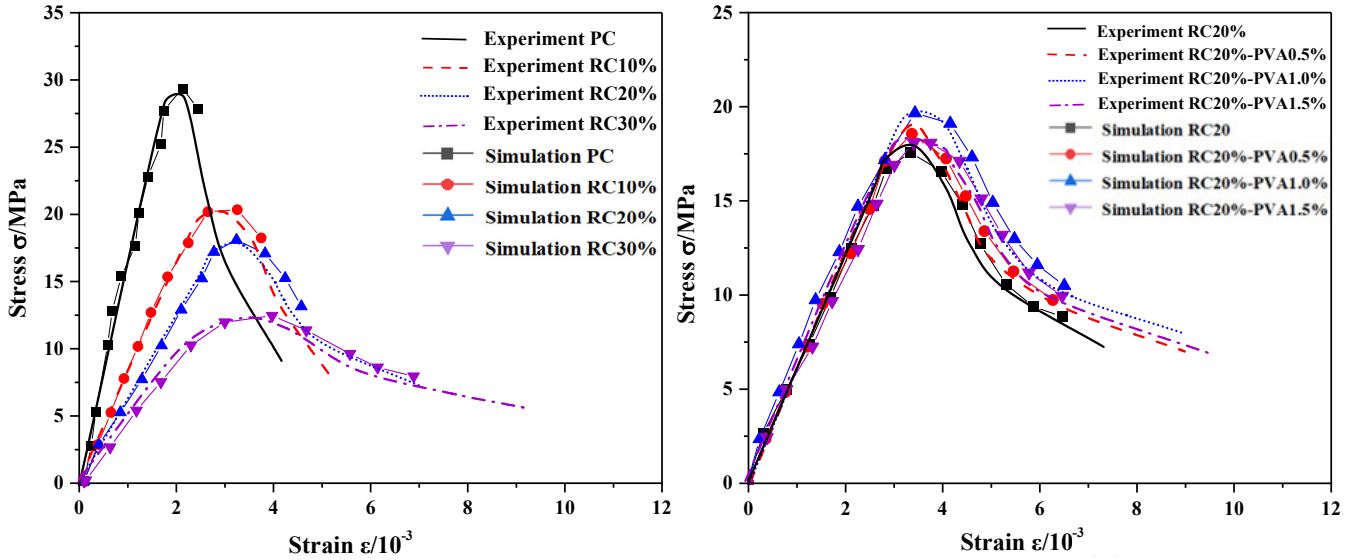

Figure 17. Comparison of experimental and simulation results.

5. Conclusions

(1) According to the test and stress–strain curve, it can be seen that when polyvinyl alcohol (PVA) fiber is mixed into rubber/concrete specimens, the failure of the specimen shows obvious ductility characteristics, and the specimen remains intact. The bridge effect of PVA and its synergistic action with rubber makes the crack width smaller, the expansion slower, and the crack zone more widely distributed, and the specimens show better axial compressive toughness. The compressive strength of PVA rubber/concrete increases with an increase in PVA content, and ductility also increases after the entire curve peak, indicating that PVA content lessens the negative impact of rubber particles on the compressive strength of concrete. The compressive strength of rubber concrete is most significantly increased when 1.0 vol%PVA is added. The cause is that high PVA content makes it simple for it to aggregate, which leads to significant interface flaws. The specimen receives insufficient opposing pressure when the PVA content is too low.

(2) It can be seen from the finite element numerical simulation that the damage first occurs at the interface, then develops into cracks, then expands and evolves to other areas, and finally reaches the failure state. Subsequently, we can seek ways to enhance the interfacial binding force to enhance the mechanical properties of the specimen.

(3) The peak compressive stress and associated peak strain of concrete diminish with an increase in rubber content, according to the results of a three-dimensional mesoscopic numerical simulation and experimental comparison, which suggests that concrete's strength declines as rubber content rises. Peak compressive stress and post-peak ductility of PVA rubber concrete rise with an increase in PVA when the rubber component remains constant, which is consistent with the actual condition.

The accuracy of the calculation model in this research is demonstrated by comparing the calculation results with the experimental data, providing a theoretical framework for the design calculation of PVA-fiber-reinforced rubber concrete. The research and development of novel materials can be sped up by numerical simulation in conjunction with essential mechanical testing, which also serves as the technical foundation for the use of new materials.

Author Contributions: Conceptualization, Y.F.; Methodology, C.Z.; Software, Z.N.; Validation, Y.F., C.Z. and L.L.; Investigation, L.L.; Resources, Y.F.; Writing—Original Draft Preparation, Z.N.; All authors have read and agreed to the published version of the manuscript.

Funding: This research was funded by the Innovative Funds Plan of Henan University of Technology: No.2020ZKCJ21/ /The Zhengzhou Collaborative Innovation Project: No. 21ZZXTCX09/ /Key scientific research projects of Henan Province colleges and universitiesin 2023: 23B570003;/ /2021 Higher Education Teaching Reform Research and Practice Project in Henan Province: 2021SJGLX670;/ /Henan Provincial Development and Reform Commission: Yufa Gaoji [2022] No. 315.

Institutional Review Board Statement: Not applicable.

Informed Consent Statement: Not applicable.

Data Availability Statement: Not applicable.

Conflicts of Interest: The authors declare no conflict of interest.

References

1. Segre, N.; Joekes, I. Use of tire rubber particles as addition to cement paste. *Cem. Concr. Res.* **2000**, *30*, 1421–1425. [CrossRef]
2. Ganjian, E.; Khorami, M.; Maghsoudi, A.A. Scrap-tyre-rubber replacement for aggregate and filler in concrete. *Constr. Build. Mater.* **2009**, *23*, 1828–1836. [CrossRef]
3. Li, G.; Stubblefield, M.A.; Garrick, G.; Eggers, J.; Abadie, C.; Huang, B. Development of waste tire modified concrete. *Cem. Concr. Res.* **2004**, *34*, 2283–2289. [CrossRef]
4. Dong, Q.; Huang, B.; Shu, X. Rubber modified concrete improved by chemically active coating and silane coupling agent. *Constr. Build. Mater.* **2013**, *48*, 116–123. [CrossRef]
5. Shu, X.; Huang, B. Recycling of waste tire rubber in asphalt and portland cement concrete: An overview. *Constr. Build. Mater.* **2014**, *67*, 217–224. [CrossRef]
6. Topçu, I.B. The properties of rubberized concretes. *Cem. Concr. Res.* **1995**, *25*, 304–310. [CrossRef]
7. Liu, S.; Zhu, D.; Li, G.; Yao, Y.; Ou, Y.; Shi, C.; Du, Y. Flexural response of basalt textile reinforced concrete with pre-tension and short fibers under low-velocity impact loads. *Constr. Build. Mater.* **2018**, *169*, 859–876. [CrossRef]
8. Ou, Y.; Zhu, D. Tensile behavior of glass fiber reinforced composite at different strain rates and temperatures. *Constr. Build. Mater.* **2015**, *96*, 648–656. [CrossRef]
9. Ou, Y.; Zhu, D.; Li, H. Strain Rate and Temperature Effects on the Dynamic Tensile Behaviors of Basalt Fiber Bundles and Reinforced Polymer Composite. *J. Mater. Civ. Eng.* **2016**, *28*, 04016101. [CrossRef]
10. Li, K.; Liu, W.; Zhang, K.; Wang, X.; Zhu, J.; Sheikh, S. Bond behavior of stainless steel wire ropes embedded in engineered cementitious composites. *Constr. Build. Mater.* **2021**, *281*, 122622. [CrossRef]
11. Zhang, K.; Yuan, Q.; Zhu, J. Analytical model for the bonding performance between HSSWM-ECC and concrete. *Cem. Concr. Compos.* **2022**, *132*, 104632. [CrossRef]
12. Zhu, J.; Zhang, K.; Wang, X.; Li, K.; Zou, X.; Feng, H. Bond-Slip Performance between High-Strength Steel Wire Rope Meshes and Engineered Cementitious Composites. *J. Mater. Civ. Eng.* **2022**, *34*, 04022048. [CrossRef]
13. Li, V.C.; Wu, C.; Wang, S.X.; Ogawa, A.; Saito, T. Interface tailoring for strain-hardening polyvinyl alcohol-engineered cementitious composite (PVA-ECC). *Aci Mater. J.* **2002**, *99*, 463–472.
14. Wang, J.; Dai, Q.; Si, R.; Guo, S. Investigation of properties and performances of Polyvinyl Alcohol (PVA) fiber-reinforced rubber concrete. *Constr. Build. Mater.* **2018**, *193*, 631–642. [CrossRef]
15. Yuan, B.; Chen, W.; Zhao, J.; Li, L.; Liu, F.; Guo, Y.; Zhang, B. Addition of alkaline solutions and fibers for the reinforcement of kaolinite-containing granite residual soil. *Appl. Clay Sci.* **2022**, *228*, 106644. [CrossRef]
16. Yuan, B.; Chen, W.; Zhao, J.; Yang, F.; Luo, Q.; Chen, T. The Effect of Organic and Inorganic Modifiers on the Physical Properties of Granite Residual Soil. *Adv. Mater. Sci. Eng.* **2022**, *2022*, 1–13. [CrossRef]
17. Yuan, B.; Chen, M.; Chen, W.; Luo, Q.; Li, H. Effect of Pile-Soil Relative Stiffness on Deformation Characteristics of the Laterally Loaded Pile. *Adv. Mater. Sci. Eng.* **2022**, *2022*, 1–13. [CrossRef]
18. Yuan, B.; Li, Z.; Chen, W.; Zhao, J.; Lv, J.; Song, J.; Cao, X. Influence of Groundwater Depth on Pile–Soil Mechanical Properties and Fractal Characteristics under Cyclic Loading. *Fractal Fract.* **2022**, *6*, 198. [CrossRef]
19. Si, R.; Guo, S.; Dai, Q. Durability performance of rubberized mortar and concrete with NaOH-Solution treated rubber particles. *Constr. Build. Mater.* **2017**, *153*, 496–505. [CrossRef]
20. Han, Q.; Yang, G.; Xu, J.; Fu, Z.; Lacidogna, G.; Carpinteri, A. Acoustic emission data analyses based on crumb rubber concrete beam bending tests. *Eng. Fract. Mech.* **2019**, *210*, 189–202. [CrossRef]
21. Masad, N.; Zollinger, D.; Kim, S.-M.; Grasley, Z. Meso-scale model for simulations of concrete subjected to cryogenic temperatures. *Mater. Struct.* **2015**, *49*, 2141–2159. [CrossRef]
22. Chen, H.; Xu, B.; Wang, J.; Zhou, T.; Mo, Y.L. Parametric analysis on compressive strain rate effect of concrete using mesoscale modeling approach. *Constr. Build. Mater.* **2020**, *246*, 118375. [CrossRef]

23. Jin, L.; Yu, W.; Du, X. Effect of Initial Static Load and Dynamic Load on Concrete Dynamic Compressive Failure. *J. Mater. Civ. Eng.* **2020**, *32*, 04020351. [CrossRef]
24. Maleki, M.; Rasoolan, I.; Khajehdezfuly, A.; Jivkov, A.P. On the effect of ITZ thickness in meso-scale models of concrete. *Constr. Build. Mater.* **2020**, *258*, 119639. [CrossRef]
25. Fuller, W.B.; Thompson, S.E. The Laws of Proportioning, Concrete. *Trans. Am. Soc. Civ. Eng.* **1907**, *59*, 67–143. [CrossRef]
26. Jin, L.; Yu, W.; Du, X.; Yang, W. Mesoscopic numerical simulation of dynamic size effect on the splitting-tensile strength of concrete. *Eng. Fract. Mech.* **2019**, *209*, 317–332. [CrossRef]
27. Wang, Z.M.; Kwan, A.K.H.; Chan, H.C. Mesoscopic study of concrete I: Generation of random aggregate structure and finite element mesh. *Comput. Struct.* **1999**, *70*, 533–544. [CrossRef]
28. Park, S.-M.; Lim, J.H.; Seong, M.R.; Sohn, D. Efficient generator of random fiber distribution with diverse volume fractions by random fiber removal. *Compos. Part B Eng.* **2019**, *167*, 302–316. [CrossRef]
29. Vaughan, T.J.; McCarthy, C.T. A combined experimental–numerical approach for generating statistically equivalent fibre distributions for high strength laminated composite materials. *Compos. Sci. Technol.* **2010**, *70*, 291–297. [CrossRef]
30. Xu, W.X.; Chen, H.S.; Lv, Z. An overlapping detection algorithm for random sequential packing of elliptical particles. *Phys. A Stat. Mech. Appl.* **2011**, *390*, 2452–2467. [CrossRef]
31. Yang, L.; Yan, Y.; Ran, Z.; Liu, Y. A new method for generating random fibre distributions for fibre reinforced composites. *Compos. Sci. Technol.* **2013**, *76*, 14–20. [CrossRef]
32. Zhu, C.; Zhu, P.; Liu, Z.; Tao, W. Numerical investigation of fiber random distribution on the mechanical properties of yarn in-plain woven carbon fiber-reinforced composite based on a new perturbation algorithm. *J. Compos. Mater.* **2017**, *52*, 755–771. [CrossRef]
33. Carreira, D.J.; Chu, K.H. Stress-strain relationship for plain concrete in compression. *J. Am. Concr. Inst.* **1985**, *82*, 797–804. [CrossRef]
34. Li, D.; Zhuge, Y.; Gravina, R.; Mills, J.E. Compressive stress strain behavior of crumb rubber concrete (CRC) and application in reinforced CRC slab. *Constr. Build. Mater.* **2018**, *166*, 745–759. [CrossRef]
35. Li, L.; Ruan, S.; Zeng, L. Mechanical properties and constitutive equations of concrete containing a low volume of tire rubber particles. *Constr. Build. Mater.* **2014**, *70*, 291–308. [CrossRef]
36. Naderi, S.; Tu, W.; Zhang, M. Meso-scale modelling of compressive fracture in concrete with irregularly shaped aggregates. *Cem. Concr. Res.* **2021**, *140*, 106317. [CrossRef]
37. Popovics, S. A numerical approach to the complete stress-strain curve of concrete. *Cem. Concr. Res.* **1973**, *3*, 583–599. [CrossRef]
38. Xiong, Q.; Wang, X.; Jivkov, A.P. A 3D multi-phase meso-scale model for modelling coupling of damage and transport properties in concrete. *Cem. Concr. Compos.* **2020**, *109*, 103545. [CrossRef]
39. Haifeng, L.; Ping, W. Dynamic characteristics of concrete with different interfacial phase thicknesses. *Chin. J. High Press. Phys.* **2017**, *31*, 249–260. [CrossRef]
40. Li, M.; Hao, H.; Shi, Y.; Hao, Y. Specimen shape and size effects on the concrete compressive strength under static and dynamic tests. *Constr. Build. Mater.* **2018**, *161*, 84–93. [CrossRef]